JOURNAL OF BIOMOLECULAR STRUCTURE AND DYNAMICS
https://doi.org/10.1080/07391102.2021.1875886

Taylor & Francis
Taylor & Francis Group

RNA dependent RNA polymerase (RdRp) as a drug target for SARS-CoV2

Avinash Mishra and Anurag S. Rathore

Department of Chemical Engineering, Indian Institute of Technology, New Delhi, India

Communicated by Ramaswamy H. Sarma

ABSTRACT

RNA-dependent RNA polymerase (RdRp), also called nsp12, is considered a promising but challenging drug target for inhibiting replication and hence, the growth of various RNA-viruses. In this report, a computational study is performed to offer insights on the binding of Remdesivir and Galidesivir with SARS-CoV2 RdRp with natural substrate, ATP, as the control. It was observed that Remdesivir and Galidesivir exhibited similar binding energies for their best docked poses, −6.6 kcal/mole and −6.2 kcal/mole, respectively. ATP also displayed comparative and strong binding free energy of −6.3 kcal/mole in the catalytic site of RdRp. However, their binding locations within the active site are distinct. Further, the interaction of catalytic site residues (Asp760, Asp761, and Asp618) with Remdesivir and Galidesivir is comprehensively examined. Conformational changes of RdRp and bound molecules are demonstrated using 100 ns explicit solvent simulation of the protein-ligand complex. Simulation suggests that Galidesivir binds at the non-catalytic location and its binding strength is relatively weaker than ATP and Remdesivir. Remdesivir also binds at the catalytic site and showed high potency to inhibit the function of RdRp. Binding of co-factor units nsp7 and nsp8 with RdRp (nsp12) complexed with Remdesivir and Galidesivir was also examined. MMPBSA binding energy for all three complexes has been computed across the 100 ns simulation trajectory. Overall, this study suggests, Remdesivir has anti-RdRp activity *via* binding at a catalytic site. In contrast, Galidesivir may not have direct anti-RdRp activity but it can induce a conformational change in the RNA polymerase.

ARTICLE HISTORY
Received 30 July 2020
Accepted 8 January 2021

KEYWORDS
SARS-CoV2; nCoV19; RNA polymerase; Remdesivir

1. Introduction

Novel coronavirus disease 2019, also known as COVID19, started in December 2019 from Wuhan, China (Zhu et al., 2020). To date, it has infected ≈ 71 million people across the globe and caused death for 1.59 million, with the numbers still growing. Across the world, many research organizations and pharmaceutical companies are engaged in designing therapeutic either in the form of treatment molecules or vaccines to control COVID19 (Diamond & Pierson, 2020). Currently, there are 100 vaccine candidates under the different stages of development and trials against SARS-CoV2. Repurposing of known drug molecules is also gaining interest amongst drug developers (Baron et al., 2020; Elfiky, 2020; Fan et al., 2020; Li & De Clercq, 2020; Zhou et al., 2020) due to shorter development time.

Many antiviral molecules have shown activity against different classes of viruses (Rolain et al., 2007; Standing, 2020; Xu et al., 2020). Remdesivir is an adenosine triphosphate analog that was first initially reported as a potential treatment for the Ebola virus (Warren et al., 2016). Later, its activity against members of the coronavirus family has also been demonstrated (Sheahan et al., 2017). Considering its antiviral property, Remdesivir is being researched as a potential treatment for COVID-19 (Ko et al., 2020; Wang et al., 2020). Remdesivir is a nucleoside analog used to inhibit the activity of RNA-dependent RNA polymerase (RdRp) enzyme of SARS-CoV2. Currently, it is allowed by the FDA for emergency practice on COVID19 critical patients (Remdesivir for Certain Hospitalized COVID-19 Patients, n.d.). Galidesivir, another nucleotide analog, initially developed against Zaire Ebolavirus (Julander et al., 2017; Tchesnokov et al., 2019) is being examined as a potential candidate against SARS-CoV2 (Westover et al., 2018). It showed positive outcomes during animal testing against various pathogens, including Ebola, Marburg, Yellow Fever, and Zika viruses. Like Remdesivir, Galidesivir also acts on the RNA dependent RNA polymerase (RdRp) (Warren et al., 2014). Other than these two nucleotide analogs, Favipiravir which is a modified pyrazine analog has also received attention for COVID19 treatment. Favipiravir has been already approved in Japan as a therapeutic for resistant cases of influenza (Furuta et al., 2017; Hayden & Shindo, 2019). It acts against RdRp enzyme (Shu & Gong, 2016) and its activity has been studied for different coronaviruses including SARS-CoV2 (Harrison, 2020).

In this study, a computational approach has been used to elucidate the atomistic level details for the binding of ATP, Remdesivir, and Galidesivir with SARS-CoV2. Initially, these two nucleoside analogues and ATP are docked with RdRp and the best-docked poses are selected for molecular

CONTACT Anurag S. Rathore asrathore@biotechcmz.com Department of Chemical Engineering, Indian Institute of Technology, Hauz Khas, New Delhi, 110016, India

Supplemental data for this article can be accessed online at https://doi.org/10.1080/07391102.2021.1875886.

dynamic (MD) simulation to determine the precise location and dynamic behaviour of ligands within the binding cavity. In addition, protein-protein interaction study of a simulated molecule of RdRp with its other co-factor units nsp8 and nsp7 is performed to evaluate its ability to form an active complex after binding with these nucleotide analogs. RdRp protein has a big binding site and this study showed interesting data points on translational and rotational movement of bound ligands within the binding cavity. Interaction energetic characteristics of catalytic residues that are responsible for the activity of RdRp are examined during the simulation. Overall, we have captured motivating factors that are responsible for the binding of Remdesivir and Galidesivir with RdRp, this can lead to the development of new antivirals targeting RNA based viruses.

2. Materials and methods

Initial 3D co-ordinates of the protein molecule are sourced from recently solved RdRp apo-protein structure in PDB: 7BTF (Gao et al., 2020). The structure is solved by electron microscopy at 2.9 Å resolution having four chains representing three units of RNA polymerase complex, these units are nsp12 (chain A), nsp7 (chain B), and nsp8 (chain C, D). Chain A represents RdRp and it is extracted from the complex and used for docking with ATP, Remdesivir and Galidesivir. As the structure does not contain any ligand so a close homologous structure of RdRp is used to define the binding cavity. RdRp of hepatitis C virus (HCV) PDB code: 3H5S (de Vicente et al., 2009) is used as a reference complex for this purpose. This structure has small molecule saccharin attached to the protein at the catalytic site. Both proteins, SARS-CoV2 RdRp and HCV RdRp are structurally aligned and saccharin from HCV RdRp is transposed to SARS-CoV2 RdRp to define its binding site. The molecular structure of Remdesivir, Galidesivir, and ATP is taken from the DrugBank database (Law et al., 2014; Wishart et al., 2018). Force field parameters are generated with the mol2 format of these molecules with CHARMM forcefield using the online SwissParam tool (Zoete et al., 2011). Docking is performed using the Autodock tool on the SAMSON interface (Morris et al., 2009), it used the Autodock Vina algorithm (Trott & Olson, 2010) for docking and ranking the poses. Superposition of SARS-CoV2 RdRp and HCV RdRp proteins placed saccharin within the SARS-CoV2 RdRp frame and atoms around 8 Å from the center of saccharin molecule are considered as active site co-ordinates. This resulted in one or more participating atoms from residues: V588, I589, G590, G616, Y617, D618, Y619, S681, S682, G683, D684, A685, T686, T687, A688, Y689, N691, L758, S759, D760, D761, A763, K798, W800, D811, F812, C813, S814 and Q815 of SARS-CoV2 can constitute the binding location for ligand molecule. The binding site residues are considered at physiological conditions. Negatively charged Aspartate is present at five positions (618, 684, 760, 761, and 811) in the binding site and all these Aspartates are deprotonated and carry a single negative charge (−1). The binding site residues are under physiological conditions, negatively charged "Aspartate (D)" is found at five sites (618, 684, 760, 761, and 811) in the binding cavity. These Aspartates are in deprotonated form to carry a single negative charge (−1). Positively charged residue, Lysine, is present at a single position (798) in protonated form and thus carries a single positive charge (+1). Overall, the binding site is negatively charged dominated due to the presence of five Aspartate residues. During docking, binding site residues are treated rigid as the flexibility is accounted during the MD simulation. A grid box is created around the identified binding site residues that cover all active atoms and allow additional space for conformational searching. Center coordinates of the box (−14.09 Å, 33.37 Å, −36.01 Å) with dimension $X = 30.84$ Å, $Y = 15$, 97 and $Z = 18.15$ Å as shown in Figure S1. Scoring in Autodock Vina is based on the interaction function calculated between each pair of atoms excluding 1–4 interactions, i.e. atoms separated by three consecutive covalent bonds. A grid box is created around the identified binding site residues that cover all active atoms and allow additional space for conformational searching. Center coordinates of the box (−14.09 Å, 33.37 Å, −36.01 Å) with dimension $X = 30.84$ Å, $Y = 15$, 97 and $Z = 18.15$ Å. Scoring in Autodock Vina is based on the interaction function calculated between each pair of atoms excluding 1–4 interactions, i.e. atoms separated by three consecutive covalent bonds. Later, the predicted free energy of binding is calculated from the intermolecular part of the lowest-scoring conformation. This docking algorithm used iterated local search global optimizer. In this algorithm, a succession of steps consisting of a mutation and a local optimization is used, with each step being accepted according to the Metropolis criterion (Trott & Olson, 2010). The exhaustiveness of the searching during docking was set to 100 to reduce the probability of not finding the global minimum of the scoring function. The number of runs is set by the exhaustiveness parameter. Here, each run during docking can produce several results where promising intermediate results are remembered. These are merged, refined, clustered, and sorted automatically to produce the final result. Finally, top 10 docked poses are generated that represent the top 10 clusters based on the binding scores. Molecular dynamic simulations of the docked complexes of RdRp are performed using GROMACS (Pronk et al., 2013) with the CHARMM27 force field (Bjelkmar et al., 2010). Hydrogen atoms are added to the RdRp protein under physiological conditions and placed in a solvated box at a 1.4 nm distance from the wall. The protein-ligand complex was energetically minimized and equilibrated under NVT and NPT ensemble for 1 ns each before 100 ns production run. During the 100 ns simulation, V-rescale temperature coupling for external heat bath with 0.1 ps time constant (Morishita, 2003) for protein and the non-protein system was used while pressure coupling was performed using Parrinello-Rahman (Parrinello & Rahman, 1981) with a time constant 2 ps, long-range electrostatic was dealt with PME. Different gromacs tools/packages are used to analyze the data generated after the production run. The clustering of structures generated during simulation is done using gromos method with RMSD cut-off 0.3 nm. MMPBSA binding free energy is calculated by 'g_mmpbsa' package. VMD

(Humphrey et al., 1996) and pymol are used for molecule visualization while the 'R' package (R Studio Team, 2018) was used for plotting graphs.

3. Results and discussions

The efficacy of Remdesivir has been recently demonstrated on SARS-CoV2 using standard potency and cytotoxicity assay on Vero E6 cell lines. The report showed that Remdesivir has EC_{50} 0.77 μM, $CC_{50} > 100$ μM. Remdesivir outperformed other inhibitors in this study including chloroquine (Wang et al., 2020). In addition to Remdesivir as a therapeutic agent, recently, BioCryst announced a randomized, double-blind, placebo-controlled clinical trial to assess the safety, clinical impact, and antiviral properties of Galidesivir in patients with COVID-19. Computational studies on these inhibitors and their binding with RdRp are also performed to strengthen the COVID19 drug design pipeline (Elfiky, 2020, 2020; Naik et al., 2020; Nguyen et al., 2020; Wakchaure et al., 2020; Wu et al., 2020). In view of these developments, this investigation was initiated to determine the atomistic level interaction details of these molecules with RdRp and with the other co-factor proteins.

3.1. RdRp protein structure

The structure of RdRp (also named as nsp12) protein has been solved complexed with nsp7 and nsp8 co-factors and sourced from protein data bank (Rose et al., 2017), PDB ID: 7BTF (Gao et al., 2020). This PDB entry has three proteins: nsp12, nsp8, and nsp7, where nps12 and nsp7 consist of single-chain while nsp8 has two chains. All these three units interact with each other where nsp12-nsp8 complex shared maximum interface surface area followed by nsp8-nsp7. In contrast, co-factor nsp7, which is the smallest subunit, shares minimal interface area with nsp12. This PDB complex does not contain any ligand/inhibitor molecule to define the reference binding cavity site. However, the catalytic domain for RdRp of SAR-CoV2 is similar to other viruses including hepatitis C and poliovirus. The longest stretch of the catalytic motif has residues 611 to 626 (TPHLMGWDYPKCDRAM). This stretch contains the critical catalytic residue Asp618, which is conserved in all other related viruses. Another motif that is the part of the catalytic domain has residues 753 to 767 (FSMMILSDDAVVCFN) containing catalytic residues Ser759, Asp760, and Asp761. The entry of the NTP substrate is channelized *via* a hydrophilic cluster containing Lys545, Arg553, and Arg555 residues (Appleby et al., 2015; Gong & Peersen, 2010; McDonald, 2013).

3.2. Protein-ligand docking

The structure of RdRp of the hepatitis C virus (HCV) is co-crystalized with a 'saccharin' inhibitor that defines its binding site (PDB ID: 3H5S) (de Vicente et al., 2009). RdRp of HCV complexed with saccharin is aligned with SARS-CoV2 RdRp to designate its binding site. The active site of RdRp SARS-CoV2 is formed by a conserved domain and showed similarity with other RdRp proteins. It is comprised of multiple motifs, the longest active site motifs are 611-TPHLMGW**D**YPKCDRAM-626 and 753-FSMMILSDDAVVCFN-767. These motifs have D618 which is conserved in viral RNA polymerases including HCV RdRp. Catalytic residues 759-SDD-761 is sandwiched between two β strands. These catalytic residues are also conserved in HCV RdRp, at the 317-GDD-319 position. Sequences of ns5b from the HCV RdRp (PDB Code: 3H5S) and nsp12 from SARS-CoV2 (PDB Code: 7BTF) are aligned using EMBOSS Needle pairwise alignment tool (as shown in Figure S2a, supplementary material). Both active site motifs showed conservation and are highlighted in Figure S2(a). Their corresponding structures are also aligned to show the structural conservation of their active sites. Figure S2(b) shows the two proteins in the same orientations, motif 1 (611–626) and motif 2 (753–767) from RdRp SARS-CoV2 and corresponding aligned residues from HCV are shown in colored format to represent the structural similarity of their active sites.zNeighbouring atoms under 8 Å from the imported ligand (saccharin) are considered as the binding site and a cubical grid box was designed that covers all these residues as explained in the method section. Remdesivir, Galidesivir, and ATP are docked in the prepared grid box using the Autodock tool of the SAMSON platform. Docking search exhaustiveness is set at 100 scales and 10 docked models were generated for each docking process. Figure S3 shows the preparation of RdRp protein-ligand docking. Ten docked poses generated by Autodock Vina are ranked as per their binding scores. These scores were calculated using the inbuilt energy function of Autodock Vina as discussed in the method section, their values are shown in Table 1. Binding free energies indicates, docked poses for a given ligand molecule are structurally different but their binding scores are highly comparable. The best binding score was exhibited by Remdesivir, −6.6 kcal/mole followed by ATP, −6.3 kcal/mole and Galidesivir, −6.2 kcal/mole. The pose where the ligand is docked at the known catalytic site of RdRp with the lowest binding free energy score is prioritized. The first docked pose of Remdesivir (−6.6 kcal/mol) and second pose of ATP (−6.6 kcal/mol) are selected based on the combined criteria of the binding score and docked location. However, Galidesivir binds at a non-catalytic site in all its poses, hence its best pose selection is based on binding score i.e. first pose (−6.2 kcal/mol).

3.3. Protein-ligand docked complex interaction

The best-docked poses for each molecule are examined for protein-ligand interaction study. The study showcases the neighbouring amino acids around the ligand molecule and highlighting the polar contacts. These polar contacts are majorly responsible for holding the ligand in the binding pocket. Figure 1 shows the interacting residues with their respective ligands.

Remdesivir is the bulkiest molecule among all the ligands examined in this study. The binding site geometry of RdRp is not symmetrical, residues are skewed to one side while the other side of the pocket is vacant (see Figure S1). Remdesivir

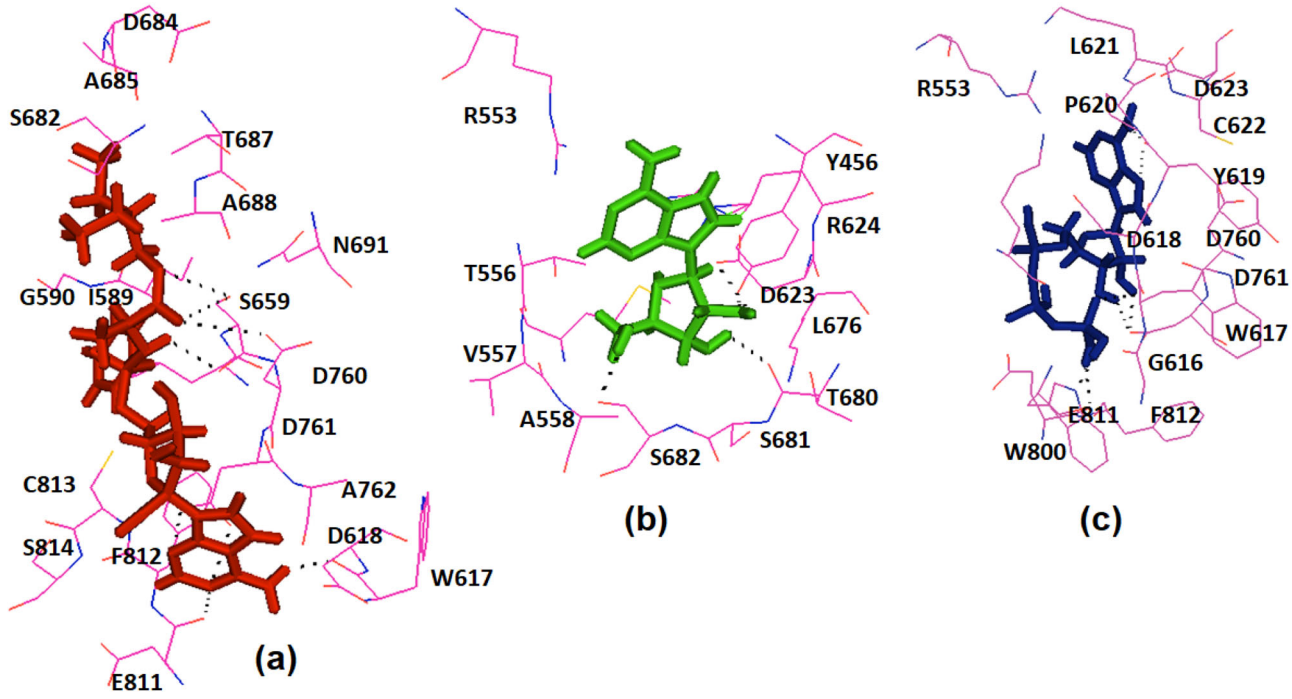

Figure 1. Neighbouring residues of (a) Remdesivir, (b) Galidesivir, (c) ATP in their best binding pose, polar contacts are highlighted, and corresponding residues are labelled.

aligns perfectly with this non-symmetrical structural characteristic of the binding site, as shown in Figure 1(a). Remdesivir's scaffold stimulates it to cover the largest surface area within the binding site. Trp617, adjacent residue to Asp618, a classic conserved residue in RdRp involved in direct polar contacts with Remdesivir while other critical catalytic residues Ser759, Asp760, Asp761 also form polar contacts with the Remdesivir. Besides, Glu811, a residue outside the catalytic domain of RdRp, makes polar interaction with the Remdesivir. Here, all the catalytic and conserved residues are involved in protein-ligand interaction. As mentioned earlier, Galidesivir binds at a non-catalytic location of the binding site. None of the critical catalytic residues of RdRp have direct polar interaction with Galidesivir. Residues, Tyr456, Thr580, Asp623, and Ser682 are involved in polar contacts (Figure 1b) with Galidesivir. Though these residues are not part of a critical catalytic site, they belong to the larger catalytic motifs of RdRp. ATP showed similar binding behavior as Remdesivir and binds in an identical orientation near to catalytic site (Figure 1c). Trp617, Tyr619, Asp761, Trp800, and Glu811, are involved in polar contacts with ATP. However, in the ATP-RdRp complex, only Asp761 from the conserved critical catalytic residue list participated in polar interaction. Overall, Figure 1 shows that the Remdesivir complex contains the maximum number of critical catalytic residues showed polar interaction and thus can strongly inhibit RdRp activity compare to ATP. In contrast, Galidesivir binds at a non-catalytic site in the binding domain and thus it may have a lesser impact on enzyme activity.

The docking protocol is formulated on the transposition of saccharin molecules from HCV RdRp. Saccharin showed a strong binding affinity with the HCV RdRp with IC50 5 nM. It has a single hydrogen bond donor while 6 hydrogen bond acceptors and formed two hydrogen bonds with HCV RdRp. Details of binding residues and type of interaction between HCV RdRp and saccharin are shown in Table S1. Catalytic residues 317-GDD-319 are placed close to saccharin in its experimental bound structure as shown in Figure 2(a). Later, this Saccharin molecule is extracted from the PDB: 3H5S and docked to SARS-CoV2 RdRp at the defined binding site to validate its resemblance with RdRp binding pattern. Docked complex of saccharin showed a high binding affinity with SARS-CoV2 similar to Remdesivir. Its best pose binds at a similar location of the binding site (shown in Figure 2b and 2c) where Remdesivir binds in its best conformation. Neighbouring residues are also showed a similar pattern. Best binding pose showed −6.4 kcal/mol Autodock Vina binding score. Binding affinity scores for the top 10 poses are shown in Figure 2(d).

3.4. MD simulation: RMSD and RMSF

Molecular dynamic simulation plays a key role in understanding the behavior of protein-ligand interaction. A sufficiently extended simulation of 100 ns is performed to find the interaction behavior of each ligand with RdRp. Before the production phase, the entire system is soaked in a water solvent and equilibrated at a given temperature and pressure. Figure 3 shows the pattern of root mean square deviation for protein and ligand among different complexes (Remdesivir, Galidesivir, and ATP). RdRp Cα atoms deviation is shown in Figure 3(a). Galidesivir showed minimum deviation with average Cα RMSD 0.37 nm. Remdesivir and ATP showed 0.43 nm and 0.46 nm average Cα RMSD. This indicates that binding of Remdesivir and ATP induced change in the protein's conformation in comparison to Galidesivir. Recently, in another study, an Apo form of SARS-RdRp is compared with bound

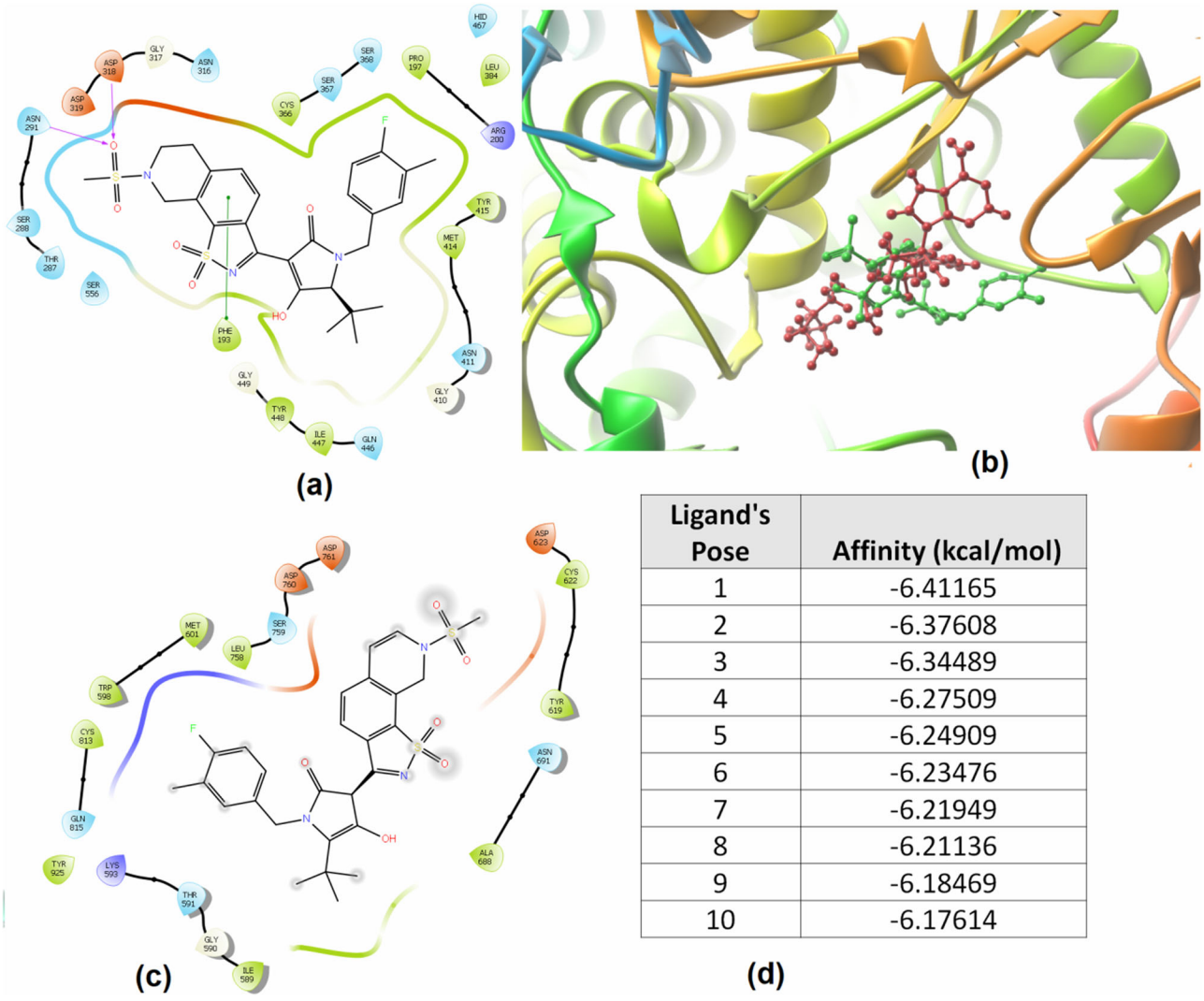

Ligand's Pose	Affinity (kcal/mol)
1	-6.41165
2	-6.37608
3	-6.34489
4	-6.27509
5	-6.24909
6	-6.23476
7	-6.21949
8	-6.21136
9	-6.18469
10	-6.17614

Figure 2. Saccharin molecule binding with HCV RdRp and SARS-CoV2 RdRp (a) interaction of HCV RdRp protein with Saccharin in experimentally bound structure, PDB ID: 3H5S, (b) best-docked pose of Saccharin (green) with SARS-CoV2 RdRp, Remdesivir best pose shown in red, (c) interaction details of best-docked pose Saccharin (green) with SARS-CoV2 RdRp, (d) Autodock Vina binding energy scores for top 10 docked poses of Saccharin with SARS-CoV2 RdRp.

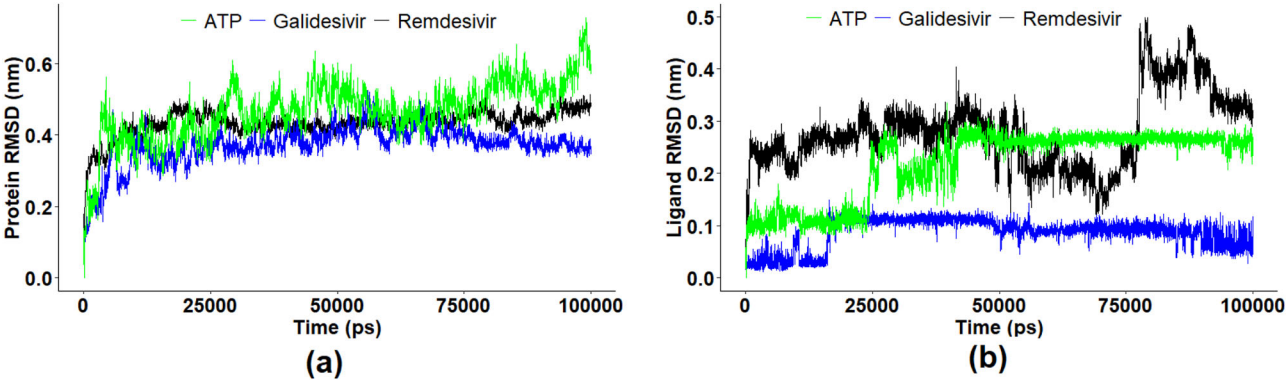

Figure 3. The behavior of protein-ligand complex during a simulation of 100 ns. (a) Cα RMSD of protein. (b) RMSD of ligands.

Remdesivir and ATP and it was found that the Apo form is much more stable while Remdesivir and ATP brought major changes in protein conformation (Arba et al., 2020). Later, the RMSD of ligands was calculated for all three complexes. Figure 3(b) shows the RMSD of ligands where ligand used as reference alignment molecule. The last 50 ns of simulation demonstrated a highly stable structural conformation for ATP and Galidesivir. Remdesivir showed a sudden spike at 75 ns and then settled down to 0.40–0.35 nm. ATP has an average deviation of 0.21 nm across the entire simulation period at

Table 1. Docking scores of Remdesivir, Galidesivir, and ATP for top 10 docked poses with RdRp SARS-CoV2.

Pose #	Remdesivir	Galidesivir	ATP
1	−6.6	−6.2	−6.3
2	−6.6	−6.1	−6.2
3	−6.5	−6.0	−6.2
4	−6.4	−6.0	−6.2
5	−6.3	−6.0	−6.1
6	−6.2	−6.0	−6.1
7	−6.2	−5.9	−6.1
8	−6.2	−5.9	−6.1
9	−6.2	−5.8	−6.0
10	−6.1	−5.7	−6.0

the binding site while Remdesivir has 0.28 nm. Galidesivir showed a very stringent conformational characteristic with an average RMSD of 0.08 nm. Data showed in Figure 3(b) indicates that ATP reached stability at ∼50 ns while Remdesivir showed some deviation in its binding behavior. In contrast, Galidesivir binds at a distant site from catalytic residue but showed the highest stability in the conformational space. Later, protein-ligand complex RMSD is also calculated. Figure S4 showed the RMSD of all three complexes using all atoms fitting. Here, ATP-complex and Remdesivir complex are invariable with average RMSD 0.5 nm and 0.47 nm. Once again, the Galidesivir protein-ligand complex has a minimum deviation. RMSD analysis shows that the Galidesivir bound system has maximum stability but it binds away from the core catalytic site. However, Remdesivir binds at the catalytic site and showed comparable stability with natural substrate ATP. It has also been shown in a similar study that Remdesivir has 100 fold better affinity than the natural substrate ATP (Zhang & Zhou, 2020). Figures 3 and S4 confirm the impact of ATP and Remdesivir at the active site of RdRp that creates a fluctuation in protein that can cause an impact on its activity.

Later, root means square fluctuation (RMSF) for each residue is averaged for all its corresponding atoms and measured for the protein RdRp. The initial stretch of residues 1–125 showed a relatively higher fluctuation of 0.6–0.75 nm. Here, the ATP complex showed marginally higher RMSF for protein than Remdesivir and Galidesivir bound protein. Residues after this stretch showed stationary behavior with RMSF $\leq$ 0.4 nm. Figure 4 shows the average RMSF of each residue for all three complexes. Fluctuation among the residues from catalytic motifs of RdRp is shown separately in Figure 4. None of these catalytic domain residues has RMSF greater than 0.25 nm for any ligand complex. Lys621 from the catalytic domain showed maximum fluctuation of 0.2 nm in Remdesivir complex followed by Ser759 in the ATP complex. RMSD and RMSF behavior of all three ligand complexes explained that they have specific binding characteristics for RdRp protein, and they remained within the binding pocket with a certain range of translation and rotational movements.

3.5. Hydrogen bonds pattern

Hydrogen bonds play a critical role in stabilizing the ligand within the protein binding pocket. H-bonds for all three ligands are measured during the simulation (Figure 5). ATP

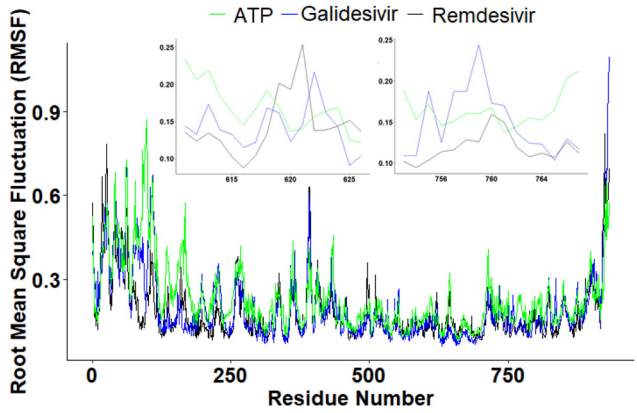

Figure 4. Root mean square fluctuation of RdRp protein among different complexes formed with ATP, Galidesivir, and Remdesivir. Catalytic residues motifs (611–626) and (753–767) are shown separately.

exhibited the highest number of hydrogen bonds, an average of 7 H-bonds with the protein in the last stable 40 ns of simulation time. Galidesivir and Remdesivir each showed an average of 2 H-bonds in this period. Overall, all three-molecules showed stable complex formation, but ATP has a maximum number of H-bonds.

3.6. Clustering

After calculating H-bonds, clustering was performed under 0.3 nm RMSD criteria on the 100 ns trajectory to find the most dominant docked conformation. Here, 2000 structures were generated during the complete simulation in different time frames. Three different groups of atoms are considered for clustering alignment: (1) protein Cα atoms (2) ligand atoms and (3) protein-ligand complex all atoms. Protein Cα atoms are aligned and clusters are formed with 0.3 nm RMSD grouping criteria. This resulted in 8 clusters in ATP bound complex while 3 and 6 for Remdesivir and Galidesivir complexes, respectively. The top cluster is composed of 87.5% of conformations in the ATP bound complex (Figure 6a). However, Remdesivir formed a maximum with 98.5% structures in its top cluster. In the case of Galidesivir, a total of 6 clusters are formed with 86.9% conformations are coming from its top cluster. Clustering based on protein Cα atoms is shown in Figure 6(a). Successively, ligand atoms are also aligned to form clusters using 0.3 nm RMSD criteria. Here, ATP and Galidesivir formed one cluster while Remdesivir formed two clusters as shown in Figure 6(b).

In ATP and Galidesivir, all conformations are grouped in one cluster while in Remdesivir 95% of structures fall in the first cluster while the rest 5% belongs to the second cluster. This indicates that ATP and Galidesivir molecules show a minimum deviation in their complexes while Remdesivir has a little deviation in its bound states. Besides, when protein-ligand complex all atoms are considered for alignment then 11 clusters are formed for ATP. Here, the cumulative deviation of protein and ligand can be observed as shown in Figure 6(c). Here again, Remdesivir has maximum conformation in its top cluster. The central structures of these clusters are considered as representative conformation and thus studied as the most dominant docked pose. This

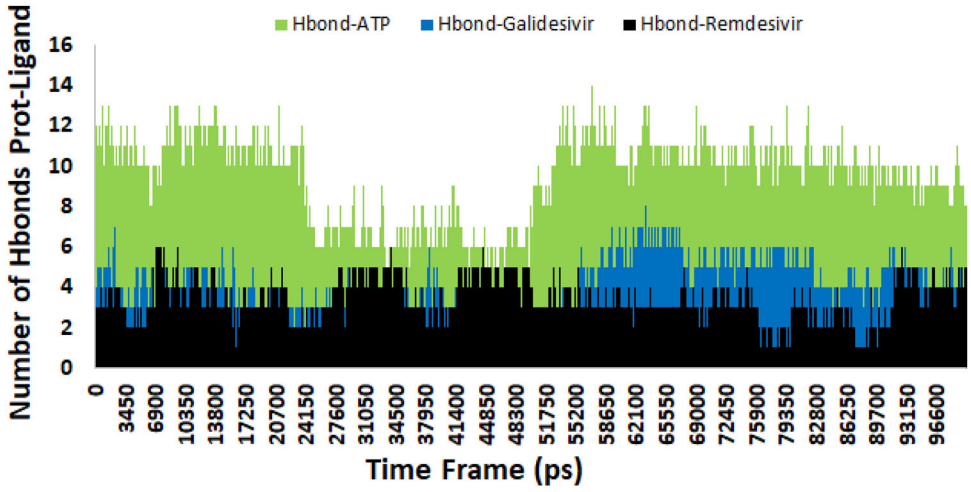

Figure 5. Hydrogen bond distribution during 100 ns simulation for ATP, Galidesivir, and Remdesivir complexes.

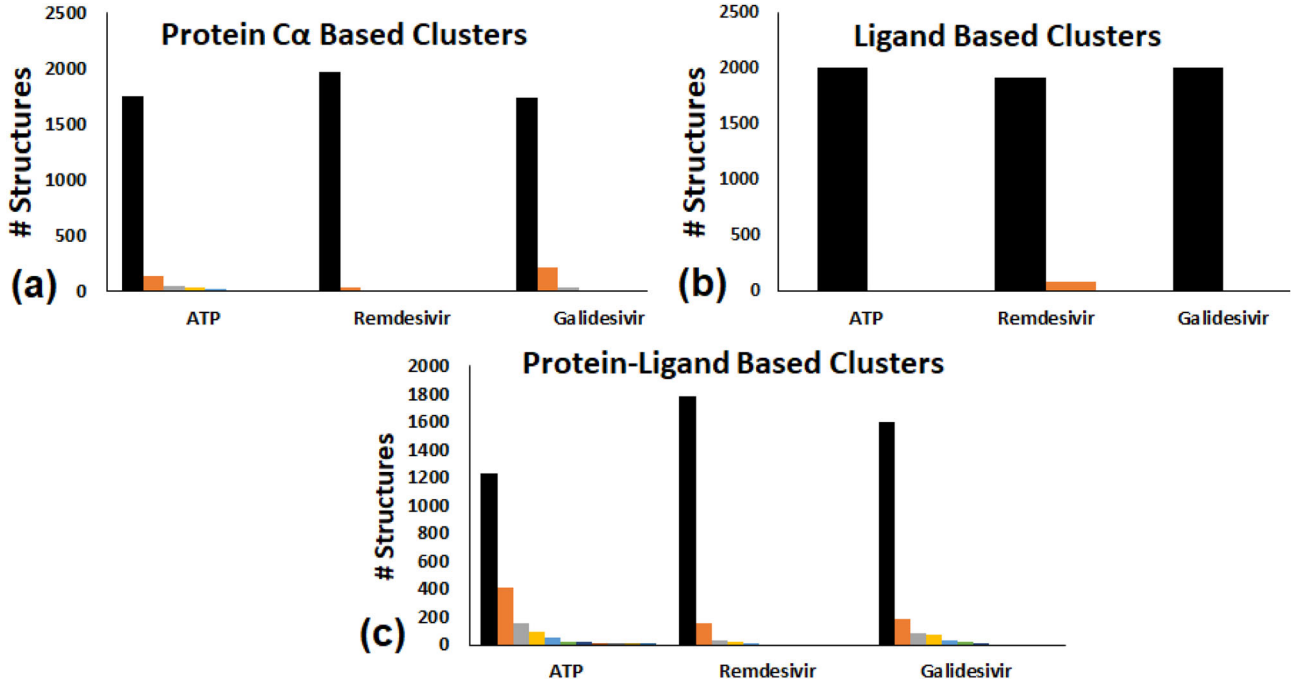

Figure 6. Clustering of simulation trajectory and their corresponding number of structures in (a) protein Cα based, (b) ligand atoms based, and (c) protein-ligand all atom-based clustering.

indicates that Remdesivir has minimum deviation and showed better performance than natural substrate ATP.

Post completing cluster analysis, we also performed RMSD distance analysis. Here, all the structures generated during the simulation were compared with the initial structure of the MD simulation. Conformations were grouped as their RMSD value to the initial structure. Figure 7 shows the frequency distribution curve based on the different bins for the RMSD of protein Cα atoms, ligand atoms, and ligand atoms when all protein atoms are aligned. The peak for protein Cα atoms frequency curve in ATP bound complex is found at the rightmost end (Figure 7a). Here, 70% of the conformations generated during the simulation are between 0.40–0.55 nm range for ATP complex. Remdesivir follows the trend after ATP where 84% conformation belongs to the 0.40–0.45 nm RMSD range. Figure 7(b) shows the frequencies when only ligand atoms are aligned. Here, ATP and Galidesivir acted more rigidly, ATP has 2 peaks where the first peak is at 0.12 nm RMSD while its second peak is at 0.27 nm. Galidesivir behaved even more stringently and showed its highest peak at 0.12 nm RMSD. Remdesivir RMSD has more standard deviation which is reflected by its widespread nature of curve in Figure 7(b). Its RMSD is evenly distributed between 0.22–0.32 nm. Figure 7(a) and 7(b) together claims that Remdesivir has the highest influence on RdRp conformation after ATP while Galidesivir has minimum effect on the protein but follows narrow distribution in its deviation.

Representative structures of these top clusters that are grouped based on protein Cα, ligand atoms, and protein-ligand atoms are shown in Figure 8. All three molecules (ATP, Remdesivir, and Galidesivir) are investigated to understand

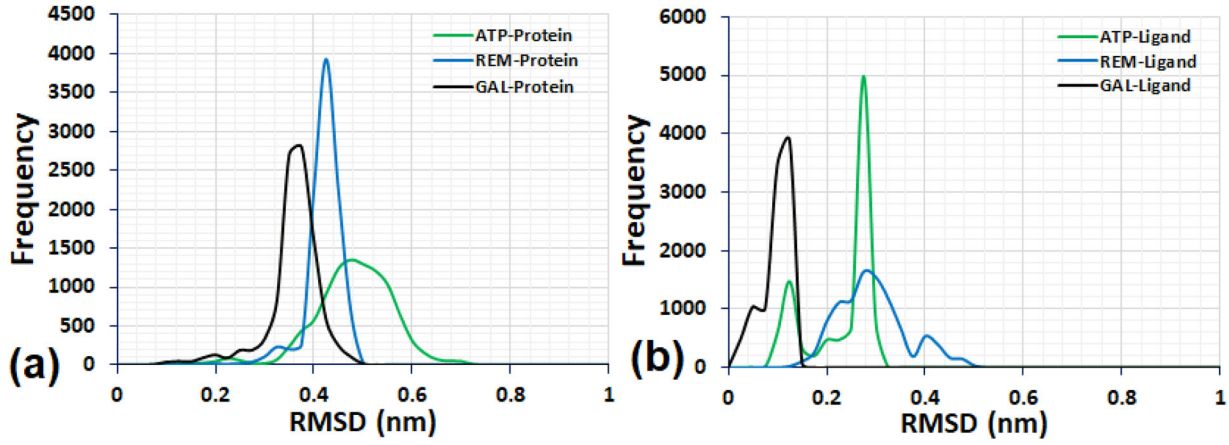

Figure 7. Frequency distribution curve for RMSD of (a) all protein Cα, (b) all atoms ligand in their ATP, Remdesivir, and Galidesivir systems.

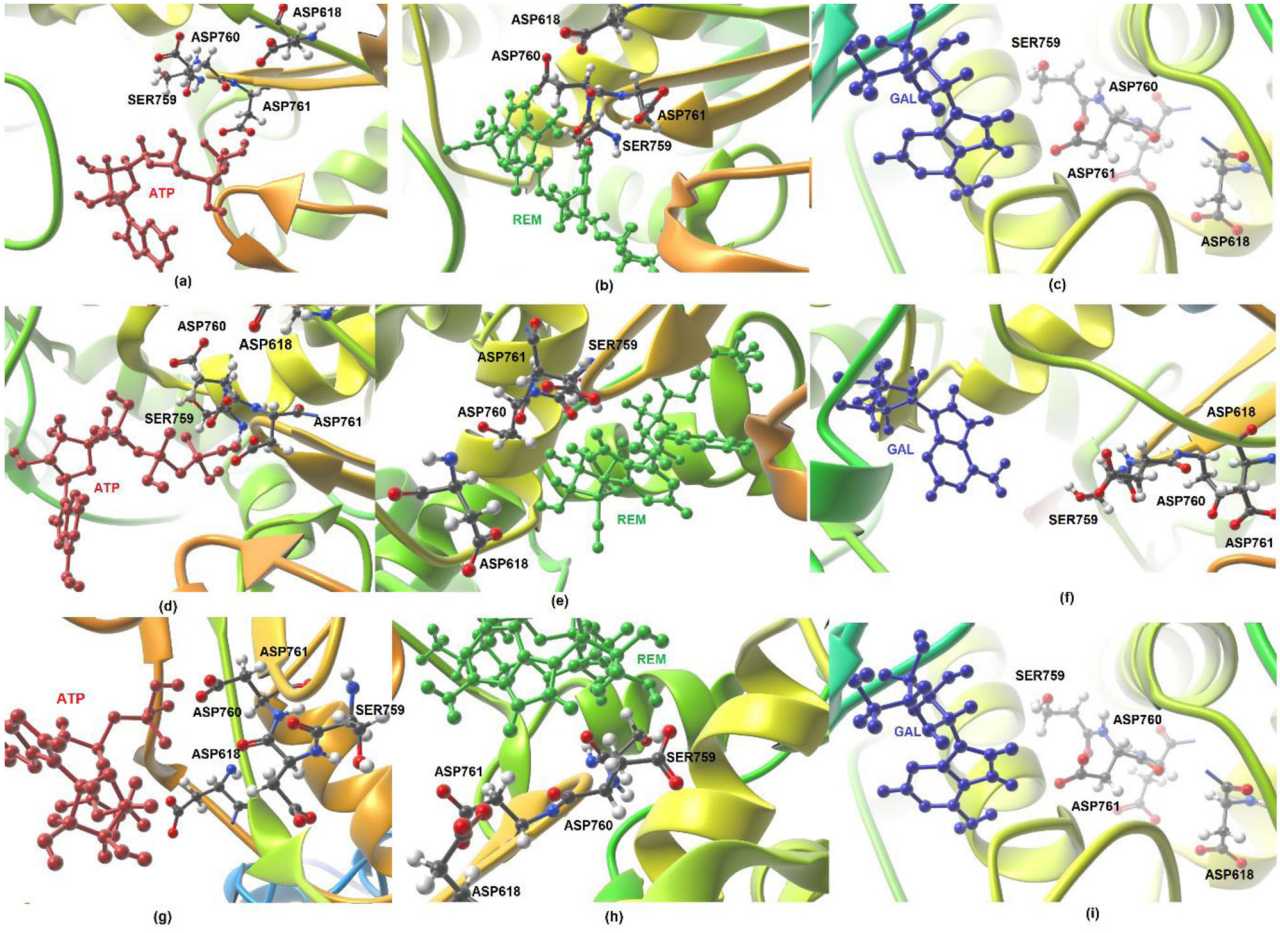

Figure 8. Spatial positioning of catalytic site (Ser759, Asp760, Asp761) residues and conserved residue (Asp618) for ATP, REM and GAL representative structure obtained from (a-c) protein Cα based, (d-f) ligand atoms based, and (g-i) protein-ligand all atom-based clustering.

the docked poses of the most populated structure in the simulation. In the ATP complex, catalytic residues (SER759, ASP760, ASP761) are close to the ligand in all three types of alignments as shown in Figure 8(a), 8(d), and 8(g). Conserved residue ASP618 also lies in the vicinity but its relative distance is larger than the catalytic residues. This indicates that ATP binds at the catalytic site of RdRp in the majority of the frames during the complete simulation. Remdesivir also follows the same pattern and is bound close to the catalytic triad as shown in Figure 8(b), 8(e), and 8(h). In contrast, Galidesivir showed the distance from these catalytic residues as shown in Figure 8(c), 8(f), and 8(i). Representative structures obtained from protein Cα atoms alignment and protein-ligand complex alignment are the same and so Figure 8(c) and 8(i) are the same. This shows that though the Galidesivir showed lesser fluctuation during the simulation (as depicted in Figure 7b) but it is bound at a relatively distant location from the catalytic and conserved residues of RdRp. This might lead to lesser activity of Galidesivir in comparison to ATP and Galidesivir. However, Remdesivir binds at the catalytic site similar to ATP with lesser fluctuation.

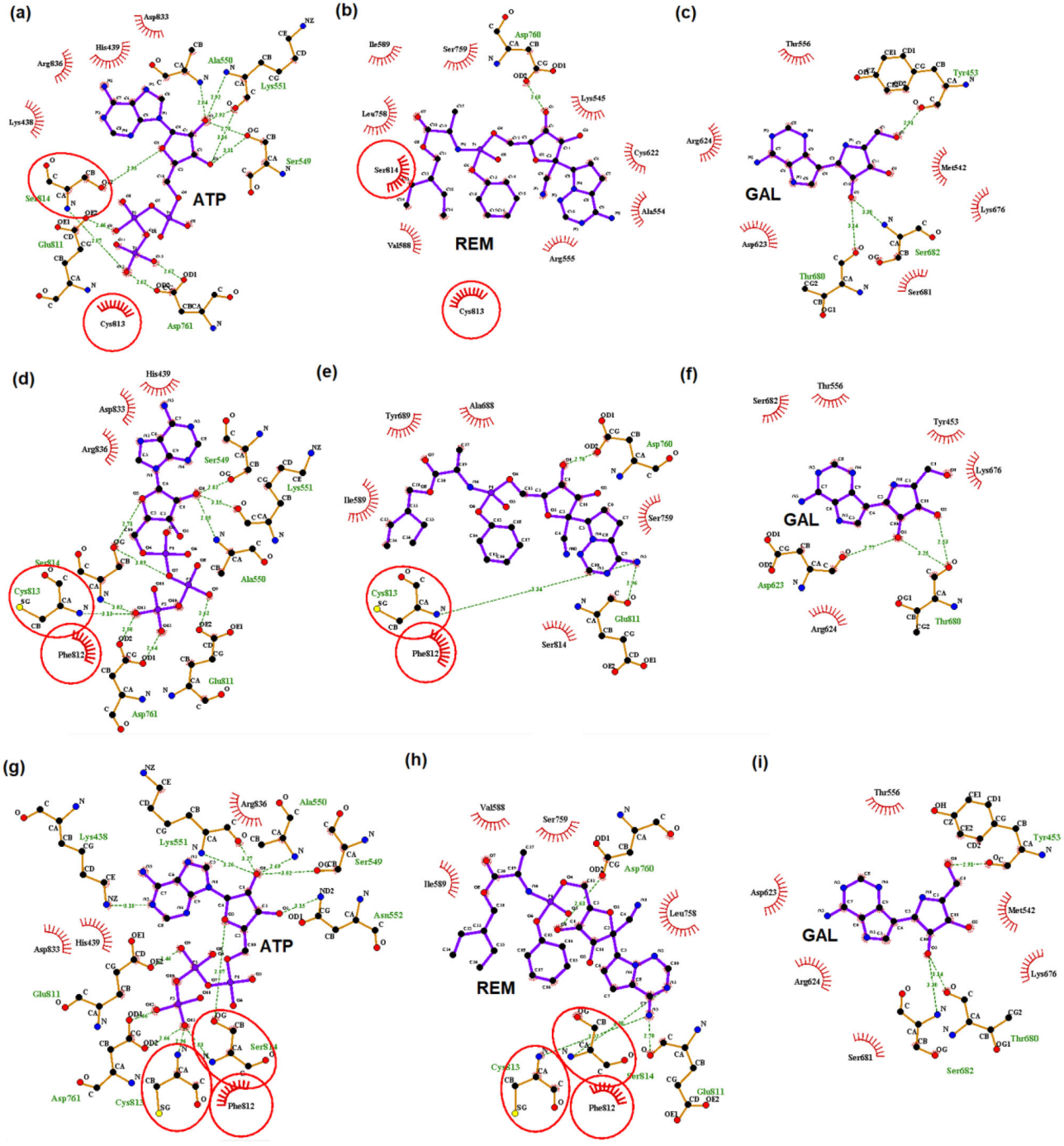

Figure 9. Protein-Ligand Interaction plots for the representative docked complex of top clusters formed for ATP, REM and GAL from (a–c) protein-based, (d–f) ligand-based, and (g–i) protein-ligand based alignment.

3.7. Protein-ligand interaction

Ligand protein interaction was detected and plotted using the LigPlot tool, all three representative structures from above top clusters shown in Figure 8 for ATP, Galidesivir, and Remdesivir complexes are used in this study. Asp761 is the core catalytic residues of RdRp are involved in H-bonding with ATP molecules in the top clusters as shown in Figure 8(a), 8(d), and 8(g). This residue plays a major role in the activity of RdRp and its interaction with ATP indicates triggering of its biological activity. Besides, Ala550, Lys551, Ser549, Ser814, Cys813 and Glu 811 also form H-bond with ATP in protein and ligand alignment cluster structure. Asn552 and Lys438 formed an additional H-bond in the protein-ligand aligned cluster structure. Remdesivir and ATP showed similar binding as shown by circled residues in their interaction plot. It forms H-bond with Asp760, a key catalytic residue in all three alignments shown in Figure 8(b) and 8(h). Similar to ATP, it also forms H-bond with Ser814, Cys813, and Glu811 in a protein-ligand based aligned cluster. As suggested earlier in this study that Galidesivir binds at a relatively distant position from core catalytic residues. Figure 8(d–f) shows that Galidesivir has no direct bonding with Ser759/Asp760/Asp761. However, it interacts with other

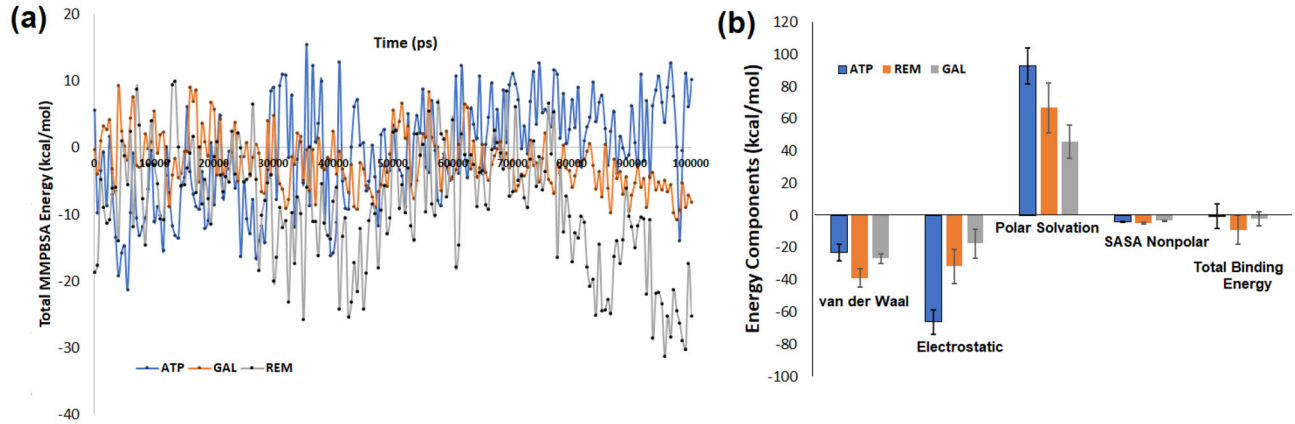

Figure 10. Energetic of RdRp protein-ligand binding (a) total MMPBSA binding free energy (kcal/mol) for three complexes over 100 ns simulation in 200 frames, (b) energy components (kcal) in binding RdRp.

residues belong to the catalytic motif. It forms H-bond with Tyr453, Asp623, Thr680, and Ser 682 residues. This interaction plot depicts that Galidesivir binds in the catalytic domain but it is placed distantly from the core catalytic residues and thus its effect on the activity of RdRp would be limited. However, Remdesivir interacts directly with the active site residue that can lead to major inhibition of RdRp activity. ATP acted as a natural substrate confirmed by its interaction with the critical residues of RdRp.

3.8. MMPBSA binding free energy

MMPBSA method is used to calculate the binding free energy between protein and ligand in their bound state. 'g_mmpbsa' is a tool developed to calculate the MMPBSA energy for the simulation trajectory. This tool is being used as an external Gromacs package. All three components (1) molecular mechanics (2) polar solvation and (3) non-polar solvation energies are calculated using this tool for the complete trajectory of the simulation for ATP, Galidesivir, and Remdesivir complexed with the RdRp protein. This tool does not calculate the entropy change component ΔS, thus the overall binding free energy has a higher magnitude. The molecular mechanics component has van der Waal and electrostatic energy calculated between protein and ligand atoms. Polar solvation energy is calculated using the Poisson-Boltzmann distribution method. However, non-polar solvation energy used the solvent-accessible surface area (SASA) method to calculate the binding free energy component.

The average values of all three MMPBSA components are calculated over the complete trajectory. Figure 10(a) shows the energy for each frame over 200 frames at 500 ps interval. The total MMPBSA average energy for the ATP complex over 100 ns of simulation is −0.52 kcal/mol. As we already mentioned, MMPBSA absolute value may not point to the experimental binding free energy due to the missing ΔS term but the negative sign indicates that the complex is stable during the simulation. Figure 10(b) shows the average energy for all its components with the standard deviation. Similarly, the average MMPBSA binding free energy for Remdesivir and Galidesivir complexes are calculated. Remdesivir has the minimum most binding free energy −8.99 kcal/mol while Galidesivir has −2.05 kcal/mol binding energies. This also showed that Remdesivir and Galidesivir bind strongly with RdRp compared to ATP. Electrostatic energy that also comprises the H-bond interaction is minimum in ATP complex which is also confirmed by the number of H-bonds during the simulation (Figure 5) but it is neutralized by high polar solvation energy. Large polar solvation term made the overall binding free energy of ATP relatively weaker. It has also been shown in an experimental study that Remdesivir has 100 fold better affinity than the natural substrate ATP (Zhang & Zhou, 2020). Combining the energetic with the position of ligands in the binding site indicates that Remdesivir binds strongly at the core catalytic site, ATP also binds at a similar location but its binding is weaker than ATP. However, Galidesivir showed binding energy stronger than ATP but it binds at a non-catalytic site.

4. Conclusions

RNA polymerase is treated as a principal target for the SARS-CoV2. Its similarity with other viruses allows us to test the existing antiviral molecule against COVID19. Nucleotide analogs, Remdesivir, and Galidesivir bind with RdRp, and investigating this *via* the *in-silico* technique is the focus of this paper. We have observed that these molecules bind efficiently with RdRp, ATP binding was also tested in this study as a reference. ATP and Remdesivir bind at the core catalytic site of RdRp while Galidesivir has a distant site of binding. Binding energies of these molecules with RdRp are highly comparable during rigid docking. However, interacting residues are quite different due to their spatial position in the binding site. RdRp has a set of residues that are labelled as critical catalytic residues. There are two catalytic motifs: residue number (611–626) and (753–767). Asp618 is the most conserved residue in viral RdRp, while Ser759, Asp760, and Asp761 are known as critical catalytic residues responsible for the activity of RdRp. In the rigid docked pose, Remdesivir forms polar contacts with three of these critical residues (Ser759, Asp760, and Asp761) while ATP showed it with only one (Asp761). Galidesivir does not have any direct polar contact with these critical residues but other residues from the

catalytic motif formed polar interaction with it. Investigating the flexibility in the docked complexes, best-docked structures are subjected to molecular dynamics simulation to understand their motion inside the binding site. RMSD value of the initial structure with all conformations generated during 100 ns simulation is similar in pattern. However, their interaction with the binding site residues is significantly varied. The representative/central structure of the most populated clusters being studied to find the compatibility of these three ligands with RdRp. Galidesivir complex showed maximum stability in terms of RMSD metric but it binds at the non-catalytic site and may not impact the activity of RdRp. However, Remdesivir binds at the core catalytic site and showed better stability than natural substrate ATP. In terms of H-bond count, ATP showed maximum H-bonds (average $\approx$ 7) during simulation while Remdesivir and Galidesivir each has an average of 7 H-bonds. However, in MMPBSA binding free energy of a complete trajectory Remdesivir showed the best binding energy due to the low solvation component which dominates the electrostatic component. The individual contribution of each residue in the binding is also calculated where ATP and Remdesivir complexes showed a high contribution of core catalytic residue in total binding free energy.

Overall, this study portrays that Remdesivir has better binding than ATP at the catalytic site of RdRp. They occupy the binding site that consists critical catalytic residues. This concludes that Remdesivir has the potential to inhibit the RdRp enzymatic activity to a significant extent *via* blocking its catalytic residues, this makes Remdesivir as potential molecule in COVID treatment (Beigel et al., 2020). However, Galidesivir binds with RdRp in the stable pose but at the non-core catalytic site. It interacts with few residues that constitute the catalytic motif of RdRp. Its binding is also confirmed by other group in their in-silico study (Elfiky, 2020). Galidesivir may not directly block the catalytic activity of RdRp but can bring conformational changes that can alter its binding with other essential co-factors (nsp7, nsp8). Thus, it could be inferred that Galidesivir can possess lower inhibitory activity against RdRp compared to Remdesivir.

Disclosure statement

No potential conflict of interest was reported by the authors.

Funding

This work was funded by the Department of Biotechnology, Ministry of Science and Technology (Grant number BT/COE/34/SP15097/2015).

ORCID

Anurag S. Rathore http://orcid.org/0000-0002-5913-4244

References

Appleby, T. C., Perry, J. K., Murakami, E., Barauskas, O., Feng, J., Cho, A., Fox, D., Wetmore, D. R., McGrath, M. E., Ray, A. S., Sofia, M. J., Swaminathan, S., & Edwards, T. E. (2015). Viral replication. Structural basis for RNA replication by the hepatitis C virus polymerase. *Science (New York, N.Y.)*, *347*(6223), 771–775. https://doi.org/10.1126/science.1259210

Arba, M., Wahyudi, S. T., Brunt, D. J., Paradis, N., & Wu, C. (2020). Mechanistic insight on the remdesivir binding to RNA-Dependent RNA polymerase (RdRp) of SARS-cov-2. *Computers in Biology and Medicine*, *129*, 104156. https://doi.org/10.1016/j.compbiomed.2020.104156

Baron, S. A., Devaux, C., Colson, P., Raoult, D., & Rolain, J. M. (2020). Teicoplanin: An alternative drug for the treatment of COVID-19? *International Journal of Antimicrobial Agents*, *55*(4), 105944. https://doi.org/10.1016/j.ijantimicag.2020.105944

Beigel, J. H., Tomashek, K. M., Dodd, L. E., Mehta, A. K., Zingman, B. S., Kalil, A. C., Hohmann, E., Chu, H. Y., Luetkemeyer, A., Kline, S., Lopez de Castilla, D., Finberg, R. W., Dierberg, K., Tapson, V., Hsieh, L., Patterson, T. F., Paredes, R., Sweeney, D. A., Short, W. R., … Lane, H. C. (2020). Remdesivir for the treatment of Covid-19 - preliminary report. *New England Journal of Medicine*, *383*(19), 1813–1826. https://doi.org/10.1056/NEJMoa2007764

Bjelkmar, P., Larsson, P., Cuendet, M. A., Hess, B., & Lindahl, E. (2010). Implementation of the CHARMM force field in GROMACS: Analysis of protein stability effects from correction maps, virtual interaction sites, and water models. *Journal of Chemical Theory and Computation*, *6*(2), 459–466. https://doi.org/10.1021/ct900549r

de Vicente, J., Hendricks, R. T., Smith, D. B., Fell, J. B., Fischer, J., Spencer, S. R., Stengel, P. J., Mohr, P., Robinson, J. E., Blake, J. F., Hilgenkamp, R. K., Yee, C., Adjabeng, G., Elworthy, T. R., Li, J., Wang, B., Bamberg, J. T., Harris, S. F., Wong, A., … Farrell, R. (2009). Non-nucleoside inhibitors of HCV polymerase NS5B. Part 4: Structure-based design, synthesis, and biological evaluation of benzo[d]isothiazole-1,1-dioxides. *Bioorganic & Medicinal Chemistry Letters*, *19*(19), 5652–5656. https://doi.org/10.1016/j.bmcl.2009.08.022

Diamond, M. S., & Pierson, T. C. (2020). The challenges of vaccine development against a new virus during a pandemic. *Cell Host & Microbe*, *27*(5), 699–703. https://doi.org/10.1016/j.chom.2020.04.021

Elfiky, A. A. (2020). Anti-HCV, nucleotide inhibitors, repurposing against COVID-19. *Life Sciences*, *248*, 117477. https://doi.org/10.1016/j.lfs.2020.117477

Elfiky, A. A. (2020). Ribavirin, Remdesivir, Sofosbuvir, Galidesivir, and Tenofovir against SARS-CoV-2 RNA dependent RNA polymerase (RdRp): A molecular docking study. *Life Sciences*, *253*, 117592. https://doi.org/10.1016/j.lfs.2020.117592

Elfiky, A. A. (2020). SARS-CoV-2 RNA dependent RNA polymerase (RdRp) targeting: An in silico perspective. *Journal of Biomolecular Structure and Dynamics*, 1–9. https://doi.org/10.1080/07391102.2020.1758790

Fan, H. H., Wang, L. Q., Liu, W. L., An, X. P., Liu, Z. D., He, X. Q., Song, L. H., & Tong, Y. G. (2020). Repurposing of clinically approved drugs for treatment of coronavirus disease 2019 in a 2019-novel coronavirus-related coronavirus model. *Chinese Medical Journal*, *133*(9), 1051–1056.

Furuta, Y., Komeno, T., & Nakamura, T. (2017). Favipiravir (T-705), a broad spectrum inhibitor of viral RNA polymerase. *Proceedings of the Japan Academy, Series B*, *93*(7), 449–463. https://doi.org/10.2183/pjab.93.027

Gao, Y., Yan, L., Huang, Y., Liu, F., Zhao, Y., Cao, L., Wang, T., Sun, Q., Ming, Z., Zhang, L., Ge, J., Zheng, L., Zhang, Y., Wang, H., Zhu, Y., Zhu, C., Hu, T., Hua, T., Zhang, B., … Rao, Z. (2020). Structure of the RNA-dependent RNA polymerase from COVID-19 virus. *Science (New York, N.Y.)*, *368*(6492), 779–782. https://doi.org/10.1126/science.abb7498

Gong, P., & Peersen, O. B. (2010). Structural basis for active site closure by the poliovirus RNA-dependent RNA polymerase. *Proceedings of the National Academy of Sciences of the United States of America*, *107*(52), 22505–22510. https://doi.org/10.1073/pnas.1007626107

Harrison, C. (2020). Coronavirus puts drug repurposing on the fast track. *Nature Biotechnology*, *38*(4), 379–381. https://doi.org/10.1038/d41587-020-00003-1

Hayden, F. G., & Shindo, N. (2019). Influenza virus polymerase inhibitors in clinical development. *Current Opinion in Infectious Diseases*, *32*(2), 176–186. https://doi.org/10.1097/QCO.0000000000000532

Humphrey, W., Dalke, A., & Schulten, K. (1996). VMD: Visual molecular dynamics. *Journal of Molecular Graphics*, *14*(1), 33–38, 27–38. https://doi.org/10.1016/0263-7855(96)00018-5

Julander, J. G., Siddharthan, V., Evans, J., Taylor, R., Tolbert, K., Apuli, C., Stewart, J., Collins, P., Gebre, M., Neilson, S., Van Wettere, A., Lee, Y.-M., Sheridan, W. P., Morrey, J. D., & Babu, Y. S. (2017). Efficacy of the broad-spectrum antiviral compound BCX4430 against Zika virus in cell culture and in a mouse model. *Antiviral Research*, *137*, 14–22. https://doi.org/10.1016/j.antiviral.2016.11.003

Ko, W. C., Rolain, J. M., Lee, N. Y., Chen, P. L., Huang, C. T., Lee, P. I., & Hsueh, P. R. (2020). Arguments in favour of remdesivir for treating SARS-CoV-2 infections. *International Journal of Antimicrobial Agents*, *55*(4), 105933. https://doi.org/10.1016/j.ijantimicag.2020.105933

Law, V., Knox, C., Djoumbou, Y., Jewison, T., Guo, A. C., Liu, Y., Maciejewski, A., Arndt, D., Wilson, M., Neveu, V., Tang, A., Gabriel, G., Ly, C., Adamjee, S., Dame, Z. T., Han, B., Zhou, Y., & Wishart, D. S. (2014). DrugBank 4.0: Shedding new light on drug metabolism. *Nucleic Acids Research*, *42*(Database issue), D1091–1097. https://doi.org/10.1093/nar/gkt1068

Li, G., & De Clercq, E. (2020). Therapeutic options for the 2019 novel coronavirus (2019-nCoV). *Nature Reviews Drug Discovery*, *19*(3), 149–150. https://doi.org/10.1038/d41573-020-00016-0

McDonald, S. M. (2013). RNA synthetic mechanisms employed by diverse families of RNA viruses. *Wiley Interdisciplinary Reviews: RNA*, *4*(4), 351–367. https://doi.org/10.1002/wrna.1164

Morishita, T. (2003). Modified velocity scaling scheme for molecular dynamics at constant temperature and/or pressure. *Molecular Simulation*, *29*(1), 63–69. https://doi.org/10.1080/0892702031000065737

Morris, G. M., Huey, R., Lindstrom, W., Sanner, M. F., Belew, R. K., Goodsell, D. S., & Olson, A. J. (2009). AutoDock4 and AutoDockTools4: Automated docking with selective receptor flexibility. *Journal of Computational Chemistry*, *30*(16), 2785–2791. https://doi.org/10.1002/jcc.21256

Naik, V. R., Munikumar, M., Ramakrishna, U., Srujana, M., Goudar, G., Naresh, P., Kumar, B. N., & Hemalatha, R. (2020). Remdesivir (GS-5734) as a therapeutic option of 2019-nCOV main protease - in silico approach. *Journal of Biomolecular Structure and Dynamics*, 1–14. https://doi.org/10.1080/07391102.2020.1781694

Nguyen, H. L., Thai, N. Q., Truong, D. T., & Li, M. S. (2020). Remdesivir strongly binds to both RNA-dependent RNA polymerase and main protease of SARS-CoV-2: Evidence from molecular simulations. *Journal of Physical Chemistry B*, 124(50), 11337-11348.

Parrinello, M., & Rahman, A. (1981). Polymorphic transitions in single crystals: A new molecular dynamics method. *Journal of Applied Physics*, *52*(12), 7182–7190. https://doi.org/10.1063/1.328693

Pronk, S., Páll, S., Schulz, R., Larsson, P., Bjelkmar, P., Apostolov, R., Shirts, M. R., Smith, J. C., Kasson, P. M., van der Spoel, D., Hess, B., & Lindahl, E. (2013). GROMACS 4.5: A high-throughput and highly parallel open source molecular simulation toolkit. *Bioinformatics (Oxford, England))*, *29*(7), 845–854. https://doi.org/10.1093/bioinformatics/btt055

R Studio Team. (2018). *Integrated development environment for R*. RStudio, PBC.

Remdesivir for Certain Hospitalized COVID-19 Patients. https://www.fda.gov/news-events/press-announcements/fda-approves-first-treatment-covid-19

Rolain, J. M., Colson, P., & Raoult, D. (2007). Recycling of chloroquine and its hydroxyl analogue to face bacterial, fungal and viral infections in the 21st century. *International Journal of Antimicrobial Agents*, *30*(4), 297–308. https://doi.org/10.1016/j.ijantimicag.2007.05.015

Rose, P. W., Prlić, A., Altunkaya, A., Bi, C., Bradley, A. R., Christie, C. H., Costanzo, L. D., Duarte, J. M., Dutta, S., Feng, Z., Green, R. K., Goodsell, D. S., Hudson, B., Kalro, T., Lowe, R., Peisach, E., Randle, C., Rose, A. S., Shao, C., … Burley, S. K. (2017). The RCSB protein data bank: Integrative view of protein, gene and 3D structural information. *Nucleic Acids Research*, *45*(D1), D271–D281. https://doi.org/10.1093/nar/gkw1000

Sheahan, T. P., Sims, A. C., Graham, R. L., Menachery, V. D., Gralinski, L. E., Case, J. B., Leist, S. R., Pyrc, K., Feng, J. Y., & Trantcheva, I. (2017). Broad-spectrum antiviral GS-5734 inhibits both epidemic and zoonotic coronaviruses. *Science Translational Medicine*, *9*(396), eaal3653.

Shu, B., & Gong, P. (2016). Structural basis of viral RNA-dependent RNA polymerase catalysis and translocation. *Proceedings of the National Academy of Sciences of the United States of America*, *113*(28), E4005–4014. https://doi.org/10.1073/pnas.1602591113

Standing, J. F. (2020). Response to: Optimizing hydroxychloroquine dosing for patients with COVID-19: An integrative modeling approach for effective drug repurposing: Quantitative clinical pharmacology input to SARS-CoV-2 therapeutics should be based on robust data. *Clinical Pharmacology & Therapeutics*, 108(1), 11–15 .

Tchesnokov, E. P., Feng, J. Y., Porter, D. P., & Gotte, M. (2019). Mechanism of inhibition of ebola virus RNA-dependent RNA polymerase by Remdesivir. *Viruses*, *11*(4), 326. https://doi.org/10.3390/v11040326

Trott, O., & Olson, A. J. (2010). AutoDock Vina: Improving the speed and accuracy of docking with a new scoring function, efficient optimization, and multithreading. *Journal of Computational Chemistry*, *31*(2), 455–461. https://doi.org/10.1002/jcc.21334

Wakchaure, P. D., Ghosh, S., & Ganguly, B. (2020). Revealing the inhibition mechanism of RNA-dependent RNA polymerase (RdRp) of SARS-CoV-2 by Remdesivir and nucleotide analogues: A molecular dynamics simulation study. *Journal of Physical Chemistry B*, *124*(47), 10641–10652. https://doi.org/10.1021/acs.jpcb.0c06747

Wang, M., Cao, R., Zhang, L., Yang, X., Liu, J., Xu, M., Shi, Z., Hu, Z., Zhong, W., & Xiao, G. (2020). Remdesivir and chloroquine effectively inhibit the recently emerged novel coronavirus (2019-nCoV) in vitro. *Cell Research*, *30*(3), 269–271. https://doi.org/10.1038/s41422-020-0282-0

Wang, Y., Zhang, D., Du, G., Du, R., Zhao, J., Jin, Y., Fu, S., Gao, L., Cheng, Z., Lu, Q., Hu, Y., Luo, G., Wang, K., Lu, Y., Li, H., Wang, S., Ruan, S., Yang, C., Mei, C., … Wang, C. (2020). Remdesivir in adults with severe COVID-19: A randomised, double-blind, placebo-controlled, multicentre trial. *Lancet (London, England)*, *395*(10236), 1569–1578. https://doi.org/10.1016/S0140-6736(20)31022-9

Warren, T. K., Jordan, R., Lo, M. K., Ray, A. S., Mackman, R. L., Soloveva, V., Siegel, D., Perron, M., Bannister, R., Hui, H. C., Larson, N., Strickley, R., Wells, J., Stuthman, K. S., Van Tongeren, S. A., Garza, N. L., Donnelly, G., Shurtleff, A. C., Retterer, C. J., … Bavari, S. (2016). Therapeutic efficacy of the small molecule GS-5734 against Ebola virus in rhesus monkeys. *Nature*, *531*(7594), 381–385. https://doi.org/10.1038/nature17180

Warren, T. K., Wells, J., Panchal, R. G., Stuthman, K. S., Garza, N. L., Van Tongeren, S. A., Dong, L., Retterer, C. J., Eaton, B. P., Pegoraro, G., Honnold, S., Bantia, S., Kotian, P., Chen, X., Taubenheim, B. R., Welch, L. S., Minning, D. M., Babu, Y. S., Sheridan, W. P., & Bavari, S. (2014). Protection against filovirus diseases by a novel broad-spectrum nucleoside analogue BCX4430. *Nature*, *508*(7496), 402–405. https://doi.org/10.1038/nature13027

Westover, J.B., Mathis, A., Taylor, R., Wandersee L., Bailey, K. W., Sefing, E. J., Hickerson, B. T., Jung, K. H., Sheridan, W.P., & Gowen, B.B. (2018). Galidesivir limits Rift Valley fever virus infection and disease in Syrian golden hamsters. *Antiviral Res.*, *156*, 38–45.

Wishart, D. S., Feunang, Y. D., Guo, A. C., Lo, E. J., Marcu, A., Grant, J. R., Sajed, T., Johnson, D., Li, C., Sayeeda, Z., Assempour, N., Iynkkaran, I., Liu, Y., Maciejewski, A., Gale, N., Wilson, A., Chin, L., Cummings, R., Le, D., … Wilson, M. (2018). DrugBank 5.0: A major update to the DrugBank database for 2018. *Nucleic Acids Research*, *46*(D1), D1074–D1082. https://doi.org/10.1093/nar/gkx1037

Wu, J., Wang, H., & Li, B. (2020). Structure-aided ACEI-capped remdesivir-loaded novel PLGA nanoparticles: Toward a computational simulation design for anti-SARS-CoV-2 therapy. *Physical Chemistry Chemical Physics*, 22(48), 28434–28439.

Xu, X., Han, M., Li, T., Sun, W., Wang, D., Fu, B., Zhou, Y., Zheng, X., Yang, Y., Li, X., Zhang, X., Pan, A., & Wei, H. (2020). Effective treatment of severe COVID-19 patients with tocilizumab. *Proceedings of the National Academy of Sciences of the United States of America*, *117*(20), 10970–10975. https://doi.org/10.1073/pnas.2005615117

Zhang, L., & Zhou, R. (2020). Structural basis of the potential binding mechanism of Remdesivir to SARS-CoV-2 RNA-dependent RNA

polymerase. *Journal of Physical Chemistry B*, *124*(32), 6955–6962. https://doi.org/10.1021/acs.jpcb.0c04198

Zhou, Y., Hou, Y., Shen, J., Huang, Y., Martin, W., & Cheng, F. (2020). Network-based drug repurposing for novel coronavirus 2019-nCoV/SARS-CoV-2. *Cell Discovery*, *6*, 14. https://doi.org/10.1038/s41421-020-0153-3

Zhu, N., Zhang, D., Wang, W., Li, X., Yang, B., Song, J., Zhao, X., Huang, B., Shi, W., Lu, R., Niu, P., Zhan, F., Ma, X., Wang, D., Xu, W., Wu, G., Gao, G. F., Tan, W., & China Novel Coronavirus Investigating and Research Team. (2020). A novel coronavirus from patients with pneumonia in China, 2019. *The New England Journal of Medicine*, *382*(8), 727–733. https://doi.org/10.1056/NEJMoa2001017

Zoete, V., Cuendet, M. A., Grosdidier, A., & Michielin, O. (2011). SwissParam: A fast force field generation tool for small organic molecules. *Journal of Computational Chemistry*, *32*(11), 2359–2368. https://doi.org/10.1002/jcc.21816